Journal of
Ceramic Science
and Technology

J. Ceram. Sci. Tech., **05** [01] 23-30 (2014)
DOI: 10.4416/JCST2013-00026
available online at: http://www.ceramic-science.com

Structural, Mechanical and Optical Properties of Nanocrystalline $(K_{0.34}Na_{0.65})NbO_{3.01}$ Thin Films Deposited by RF Sputtering

P. Mahesh[1], D. Pamu*[1]

[1]Department of Physics, Indian Institute of Technology Guwahati, Guwahati – 781039, India.
received October 15, 2013; received in revised form December 11, 2013; accepted January 14, 2014

Abstract

$(K_{0.34}Na_{0.65})NbO_{3.01}$(KNN) thin films were deposited at ambient temperatures by means of RF magnetron sputtering. The X-ray diffraction patterns (XRD) reveal that the as-deposited films are amorphous and on annealing at 500 °C for 1 h induced nanocrystallinity with improved microstructure and optical properties. The crystallite size in the films varies between 44 and 20 nm and is dependent on both O_2 SCCM and the thickness of the films. The annealing process increased the grain size along with the roughness in the films. It is observed that the amorphous films exhibited higher band-gap energies (3.5 – 3.9 eV) and lower refractive indices (1.82 – 2.01 at 600 nm). On the other hand, the annealed films exhibited smaller band-gap energies (3.46 – 3.78 eV) and higher refractive indices (1.88 – 2.13 at 600 nm), which is attributed to the improvement in the crystallinity and microstructure of the films. Further, the hardness (1.54 – 10.74 GPa) and elastic modulus (17.8 – 80.3 GPa) are significantly affected by the O_2 SCCM and annealing temperature. It is found that both the optical and mechanical properties of the KNN films are profoundly influenced by the crystallinity, average particle sizes, packing densities and O_2 SCCM.

Keywords: Thin films, crystal structure, X-ray diffraction, optical properties, mechanical properties

I. Introduction

Lead-based piezoelectric ceramics are regarded as leading piezoelectric materials due to their significant properties and comparatively low processing cost [1,2]. Despite their excellent piezoelectric properties, one of the major disadvantages of lead-based ceramics is the potential lead volatility at higher temperatures. It is known that lead poisoning can result in adverse effects on health such as reduced IQ, slowed body growth, and kidney damage [3]. Hence, in the recent past there has been a search to find a suitable replacement for lead-based piezoelectric ceramics. $(K_{0.5}Na_{0.5})NbO_3$ (KNN)-based piezoelectric ceramics have attracted wide attention on account of their promising piezoelectric properties compared to other lead-free ceramics and broad operating temperature range. KNN is a solid solution of ferroelectric $KNbO_3$ and anti-ferroelectric $NaNbO_3$ [4].

In addition, the rapid development in the optoelectronics industry has greatly increased the demand for optical thin films. Ferroelectric materials are crucial to many modern technologies, in particular, piezoelectric actuators and electro-optic modulators. KNN in particular is one of the most extensively studied lead-free piezoelectric materials. However, research on KNN for integrated optical applications remains sparse. On the other hand, dielectric thin films have attracted more attention owing to their use in various applications such as microwave integrated circuits, integrated optical devices, optical coatings, anti-reflection coatings and buffer layers for growing semiconductors [5–8]. Stacks of high-index and low-index films coated alternatively have been employed in multilayer structures to enhance the performance and efficiency of optical devices. The breakdown of any such device is determined mostly by the failure of any of the layers and the degradation in its properties. Therefore, it is important to study the properties of a single-layer oxide film, which is as significant as studying the multilayer. There have been a number of studies on dielectric, piezoelectric, mechanical and electrical properties on the bulk and thin film of this material [1, 2, 4, 9–11]. Further, $(K_xNa_{1-x})NbO_3$ shows three phase boundaries for x = 0.17, 0.35 and 0.5, respectively [12]. However, most of this work has been focused on the x = 0.5 and the piezoelectric properties appear optimum when the ratio of Na/K is 50/50. Further, the literature related to the other two-phase boundaries x = 0.17, 0.35 is sparse. Mgbemere *et al.* [13] and Zang *et al.* [14] reported on the dielectric and piezoelectric properties of $(K_{0.35}Na_{0.65})NbO_3$ ceramics. However, there have been no reports on the optical and mechanical studies of $(K_{0.35}Na_{0.65})NbO_3$ in thin film form, which motivated us to pursue this study. We are therefore reporting on the structural, microstructural, optical and mechanical properties of nanocrystalline $(K_{0.35}Na_{0.65})NbO_3$ thin films deposited at ambient temperatures by means of RF magnetron sputtering. The films were deposited at different oxygen gas pressures in standard cubic centimeters per minute (SCCM) and post annealing at 500°C.

* Corresponding author: pamu@iitg.ernet.in

II. Experimental

The KNN sputtering target was prepared with the conventional solid-state reaction method from individual high-purity powders (> 99.99 %) of K_2CO_3, Na_2CO_3, and Nb_2O_5. To account for the loss of Na and K, 1 wt% of extra Na_2CO_3 and K_2CO_3 were added. The starting materials were mixed in accordance with the desired stoichiometry of the KNNceramics. A planetary ball mill (Fritsch GmbH, Germany) was used to prepare the powders. The calcined powders were ground again for 10 h. The powders were then uniaxially pressed to produce the KNN target measuring 56 mm in diameter and sintered at 900 °C for 3 h. The films were deposited at ambient temperatures on SiO_2 substrates at different O_2 SCCM and at a fixed power of 70 W for 3 h under the sputtering gas pressure of 35 m Torr. Initially, the KNN thin films were deposited at different O_2 SCCM for a constant duration of 3 h. Afterwards, the thicknesses of the films was calculated using the envelop method and verified with a stylus profiler. Subsequently, we were able to estimate the sputtering rate at different O_2 SCCM. In order to get the same order of thickness in all the films deposited at distinct O_2 SCCM, this sputtering rate was optimized.

The crystal structure and phase purity of the target material and the deposited thin films were analyzed with an X-ray diffractometer (Rigaku, TTRAX). The chemical composition of the thin films was analyzed with a scanning electron microscope (Leo 1430vp) equipped with energy dispersive spectroscopy (EDS). Spectral transmission characteristics in the wavelength range 200 – 1400 nm were measured with a UV–VIS–NIR spectrophotometer (UV 3101PC, SHIMDZU). The optical constants were calculated using the envelope technique [15]. Photoluminescence measurements were performed at room temperature with a thermo-spectronic double monochromator coupled to a GaAs photomultiplier with a conventional photon counting system (AMINOCO-Bowman-2). Mechanical properties such as elastic modulus and hardness were measured using a nanoindenter (CETR-UMT-2). The Oliver – Pharr standard method was used to calculate the composite hardness and elastic modulus.

$$H=\frac{P_{max}}{A} \quad (1)$$

$$E_r=\frac{\sqrt{\pi}S}{2\beta\sqrt{A}} \quad (2)$$

where P_{max} is the peak indentation load, A is the projected area of contact under load, β is a constant that depends on the geometry of the indenter tip, and S is the experimentally measured contact stiffness.

III. Results and Discussions

(1) Crystallinity of the KNN target and thin films

Fig. 1 shows the XRD pattern of the KNN sputtering target and along with the films annealed at 500 °C and deposited under different O_2 SCCM. The XRD pattern of the target clearly indicates the single-phase formation of KNN phase without any impurities. All the as-deposited films were found to be structurally amorphous and became partially crystalline after the post-deposition annealing. Because it is known that the oxide thin films naturally grow in the amorphous state, the activation energy is given either in the form of temperature or ion bombardment to initiate the crystal growth [16]. In other words, the presence of diffraction peaks can be used to evaluate the structural order over a long range of the material. On annealing at 500 °C, all the films were crystallized to a perovskite structure with $K_2Nb_6O_{16}$ as secondary phase. Since no split in the peaks is observed, the XRD patterns were indexed as pseudo cubic structure. Further, with an increase in O_2 SCCM, the intensity of (001) peak increases whereas the intensity of (101) peak decreases, and is attributed to the lower surface energy of (001) plane [17]. The formation of $K_2Nb_6O_{16}$ phase is expected because Na_2O is more volatile when compared with K_2O [18]. Further, the formation of $K_2Nb_6O_{16}$ (JCPDS file 28 – 0788)is expected because $K_2Nb_6O_{16}$ forms at lower temperatures compared to pure KNN. In addition, it is known to form the (Na, K)Nb_8O_{21} as secondary phases in the KNN-based ceramics and thin films owing to the volatization of K and Na. Moreover, it has also been observed that K-rich films form the $K_2Nb_6O_{16}$ whereas Na-rich films form the $Na_2Nb_6O_{16}$ as a secondary phase [19]. Besides, the formation of secondary phases depends upon the deposition technique, surface free energy of the substrate and the deposition and annealing temperatures. The weight percentage of the secondary phase is calculated using the following expression

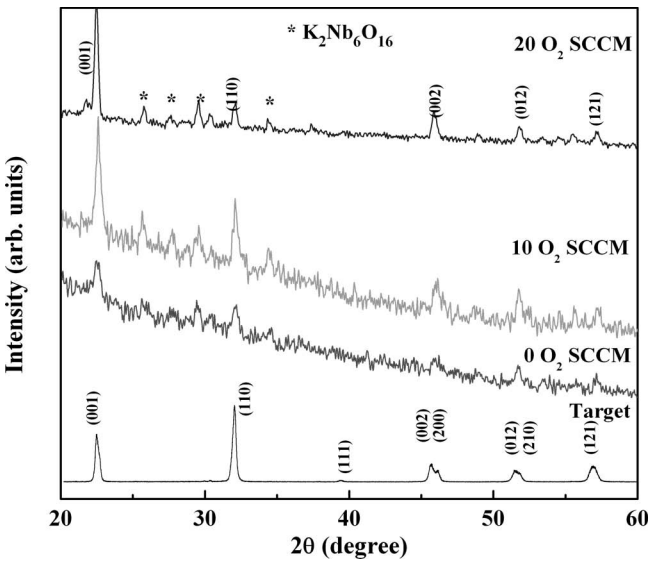

Fig. 1: XRD pattern of the KNN sputtering target and films annealed at 500 °C, deposited at different O_2 SCCM.

$$W_A=\left\{\frac{1}{\left[1+1.265\left(\frac{I_B}{I_A}\right)\right]}\right\}\times 100 \quad (3)$$

where I_A and I_B denote the intensities of the strongest reflections of $K_2Nb_6O_{16}$ and KNN phases, respectively. The weight percentage of the $K_2Nb_6O_{16}$ phase is calculated and is in the range of 3 – 5 %. Further, it is also observed that the intensities of all the KNNpeaks enhance gradually with increasing O_2 SCCM, which shows the improvement in crystallinity in the films. Furthermore, it indicates that larger-sized crystal grains and a lower concentration

of crystal defects are present in the annealed films. This mechanism occurs as a result of grain boundary motion owing to a reduction in the total boundary surface energy. The improvement in crystallinity of KNN films with an increase in O_2 SCCM can be explained as follows: during the deposition, it is possible that energy exchange and heat generation originating from the oxidation of species assisted the crystallization of KNN films, and then resulted from the formation of high-quality films upon annealing. Further, when oxygen was introduced into the chamber, the sputtered species reacted with oxygen molecules to cause heat generation and energy redistribution on the surface to the substrate; at the same time this process would promote migration and crystallization of the sputtered species. Interestingly, the films exhibited better crystallinity at lower annealing temperatures when compared with the available literature [20–22]. The average crystallite size of the films was estimated using Scherrer's method and the average crystallite size increases from 20 ± 4 to 44 ± 4 nm linearly with an increase in O_2 SCCM.

The surface morphology of the as-deposited and annealed film deposited at 10 O_2 SCCM is shown in Figs. 2a and 2b, respectively. The as-deposited films show very small shallow dimples on the surface without distinct grains and with an average grain size of 15 nm. It is interesting to note that on annealing the morphologies of all the samples become highly densified with a homogeneous distribution of particles. The surface morphology of the as-deposited films is smooth while the annealed films show an enhancement in grain growth owing to the crystallization and hence these films exhibit the denser microstructure. The average grain size of 180 nm is obtained for the film deposited at 10 O_2 SCCM. The improvement in the microstructure and average grain size can be correlated to the annealing effect, which improves the nucleation, grain growth and packing density. To confirm the stoichiometry of the films, EDAX analysis was performed on the film deposited at 10 O_2 SCCM. It was found that the composition of the films almost achieved the target composition. The obtained stoichiometry of the films is $(K_{0.34}Na_{0.65})NbO_{3.01}$ and the details of the elemental percentages are tabulated in Table 1.

(2) Optical properties

Fig. 3 shows the optical transmittance spectra of as-deposited and annealed KNN films deposited under different O_2 SCCM. It is observed that the as-deposited films are more transparent compared with the annealed films owing to the absence of scattering grain boundaries. The transmittance of all the films is around 90 % in the region above the band-gap energy. The transmittance peak coincides with the transmittance of the substrate, which indicates that good optical films are formed. All the transmission spectra show interference fringes which originate owing to interference at the air and substrate-film interfaces. The sharp fall in transmission and disappearance of fringes at shorter wavelength is due to fundamental absorption of the films.

Table 1: The required and obtained percentages of elements in KNN film deposited at 10 O_2 SCCM.

Element	Required atomic percentage	Obtained atomic percentage
K	7	6.91
Na	13	13.04
Nb	20	19.98
O	60	60.07

The obtained composition is $(K_{0.34}Na_{0.65})NbO_{3.01}$

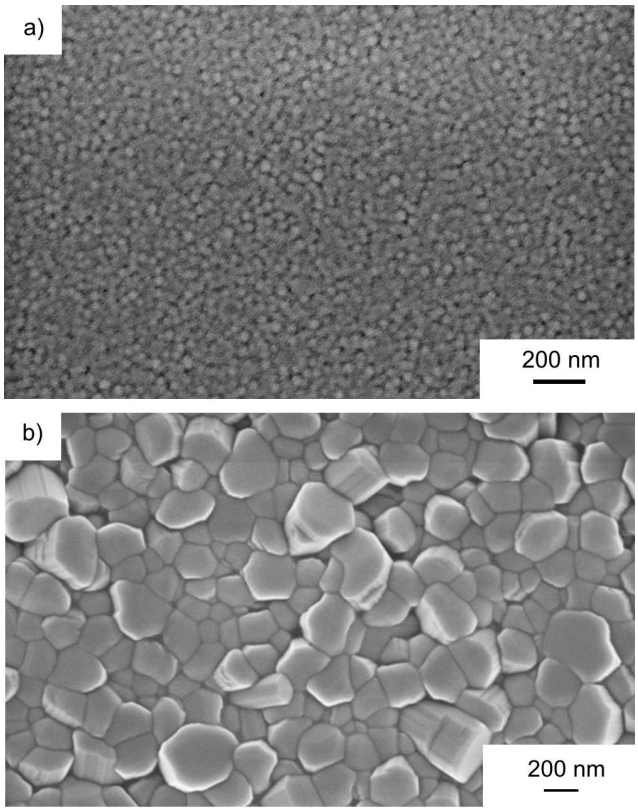

Fig. 2: (a) Surface morphology of the as-deposited film with film thickness 300 nm deposited at 10 O_2 SSCM (b) Surface morphology of the annealed film with film thickness 280 nm deposited at 10 O_2 SCCM.

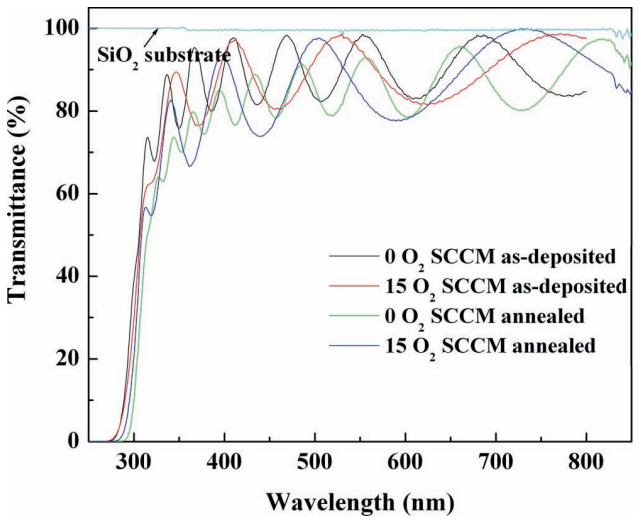

Fig. 3: The optical transmittance spectra for as-deposited and annealed KNN films deposited at different O_2 SCCM.

The refractive index (n) of the film is derived by employing the envelope method [15] based on the following expressions:

$$n = \left[N + \left(N^2 - n_S^2\right)^{0.5}\right]^{0.5} \quad (4)$$

where,

$$N = 2n_S^2\left(\frac{T_{max} - T_{min}}{T_{max}\,T_{min}}\right) + \frac{n_S^2+1}{2} \quad (5)$$

T_{max} and T_{min} are the corresponding transmittance maximum and minimum at a certain wavelength λ, and n_s is the refractive index of the substrate used. If n_1 and n_2 are the refractive indices of two adjacent maximum or minimum at wavelengths λ_1 and λ_2, then the thickness of the films (d) can be calculated with the following expression:

$$d = \frac{\lambda_1\lambda_2}{2(\lambda_1 n_2 - \lambda_2 n_1)} \quad (6)$$

$$P = \left(\frac{n_f^2-1}{n_f^2+2}\right)\left(\frac{n_b^2+2}{n_{b2}-1}\right) \quad (7)$$

Also, the optical packing density (P) of the films is calculated using the relation,

where n_b is the bulk refractive index (2.2) of KNN [23] and n_f is the observed film refractive index. The thicknesses of the deposited films are in the range of 300 – 500 nm.

Figs. 4a and 4b illustrate the variation in the refractive index (n_{600}, λ = 600 nm) and packing densities of the as-deposited and annealed films as a function of O_2 SCCM, respectively. It is observed that the refractive index of the films increased with an increase in O_2 SCCM both in the as-deposited and annealed films. Further, the annealed films exhibited higher values of refractive index compared to the as-deposited films. The values obtained for the refractive index ranged between 1.82 – 2.01 and 1.88 – 2.13 at 600 nm in the dispersion-free region, while the optical packing density values ranged between 0.77 – 0.89 and 0.81 – 0.96 for the as-deposited and annealed films, respectively. Interestingly, both the refractive index and packing density of the films show similar variation with O_2 SCCM, which can be attributed to the increase in the crystallinity and improvement in the microstructure (Fig. 2b). In addition, the low values of n observed for the as-deposited films can be correlated to the amorphous nature of the films and low adatom mobility at the ambient temperatures. Furthermore, the as-deposited films are highly disordered owing to their amorphous nature, resulting in lower film density, which in turn leads to the lowering of the refractive index. Upon annealing, there is a reduction in inter atomic spacing, resulting in the densification of the films (porosity decreases), which leads to an increase in the refractive index, and it can also be correlated to the film packing density, microstructure and crystallinity. The extinction coefficient is the fraction of light lost in scattering and absorption per unit distance in a participating medium indicates low loss. The extinction coefficients of the as-deposited and annealed films were estimated, and the values are in the order of 10^{-3} to 10^{-4}, which shows that these films exhibit low optical loss.

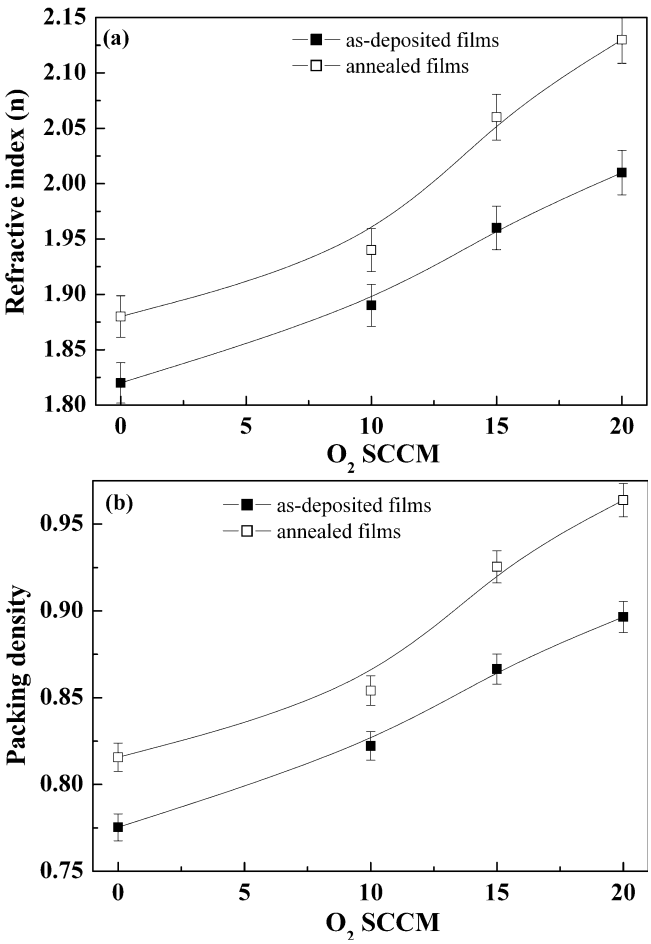

Fig. 4: (a) Variation in the refractive index of as-deposited and annealed films as a function of O_2 SCCM.(b) Variation in the packing density of as-deposited and annealed films as a function of O_2 SCCM.

The optical band-gap energy values are a good qualitative estimation of stoichiometry. The optical band-gap energy (E_g) for all the films was calculated using the Tauc relation [24], which is given by $ahv = \beta(hv - E_g)^n$, where hv is the photon energy, β is a constant, which is a measure of crystalline order in the deposited films. In the present case, the band-gap energy (E_g) was estimated by assuming an allowed indirect (n = 2) electronic transition between the highest occupied state of the valence band and the lowest unoccupied state of the conduction band. The variation in the optical band-gap energy of as-deposited and annealed films as a function of O_2 SCCM is shown in Fig. 5a. It can be seen that the optical band-gap energy of the films decreased with O_2 SCCM. The band-gap energy of the as-deposited films was in the range of 3.5 – 3.9 *eV*, which decreased to 3.46 – 3.78 *eV* for the annealed films. The absorption edges of the as-deposited and annealed film deposited at 20 O_2 SCCM are shown in Fig. 5b. The decrease in optical band-gap energy with annealing may be attributed to the increase of intermediary energy levels within the band-gap energy, the increase in crystalline nature and improvement in the surface morphology of the films, which are confirmed from the XRD patterns and SEM images, respectively. Moreover, the annealed films exhibited a red shift in the optical spectrum, which confirms the reduction in the band-gap energy of the annealed films.

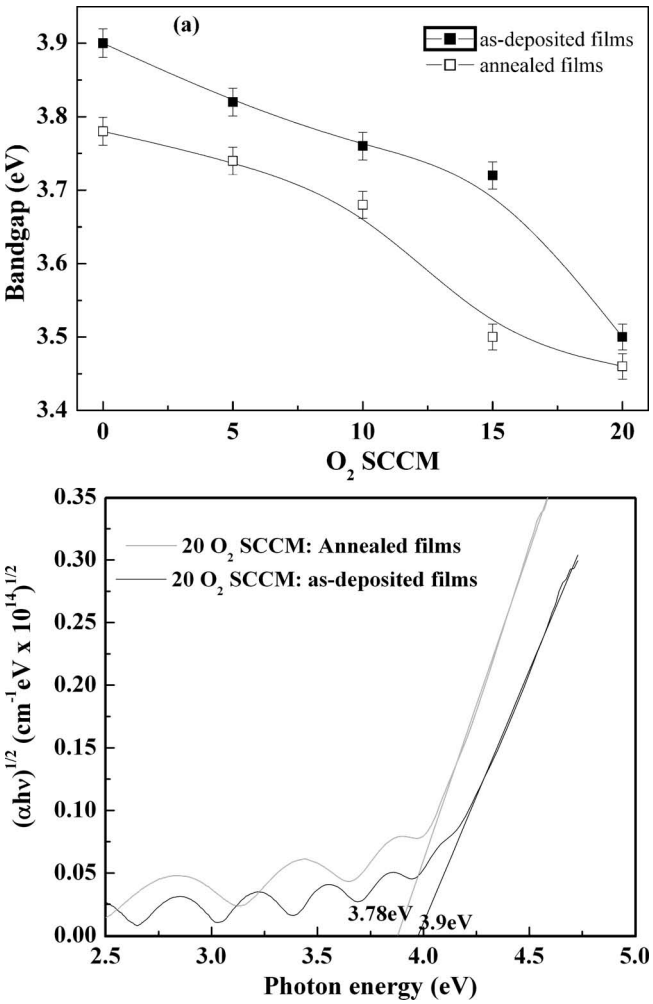

Fig. 5 : (a) Variation in the optical band-gap energy of as-deposited and annealed KNN films as a function of O_2 SCCM. (b) Absorption edges of as-deposited and annealed film deposited at 20 O_2 SCCM.

(3) Photoluminescence studies

Photoluminescence (PL) is the spontaneous emission of light from a material under optical excitation. The intensity of the PL signal provides information on the quality of surfaces, interfaces and optical band gap energy. The PL spectra of the KNN thin films were measured at room temperature in the wavelength range of 300 – 550 nm with the excitation wavelength 280 nm. Fig. 6 illustrates the PL spectra of annealed films deposited under different O_2 SCCM. All the PL spectra of the films exhibit a characteristic peak at around 360 nm, which corresponds to the near shortest visible blue emission. Furthermore, the characteristic peak of the films exhibits a slight shift in the peak position with the variation in O_2 SCCM. This can be correlated to the grain growth in the films. It is well-known that the PL peak intensity, peak width and frequency shift are strongly dependent on the film density. With increasing O_2 SCCM, the particle size becomes larger and the ratio of the surface area to volume decreases, leading to a reduction in oxygen vacancies of the films. Hence, the films tend to be more compact with fewer defects, which cause the decrease in intensity and line width. The PL study complemented the optical studies of the KNN films.

Nevertheless, it is well known that the optical properties of the films are generally related to the grain size and defects in the films. In particular, the latter may evolve owing to (i) lattice mismatch between the substrate and the films, (ii) inter diffusion of atoms between the substrate and film, (iii) deficiency of oxygen vacancy, and (iv) deviation in the stoichiometry. The lattice mismatch induces strain owing to the formation of misfit dislocations, while the inter diffusion of atoms occurring generally at the high processing temperatures leads to the formation of point defects at the interface. However, it may be noted that the contribution of point defects may be negligible as the presently investigated films were annealed only at 500 °C. Similarly, the presence of oxygen vacancies in the films reduces the optical band gap. However, the obtained EDS analysis of the investigated samples reveals that the deposited films were significantly free from oxygen vacancies. Another source of the defects is the stacking faults caused by the considerable deviations in the stoichiometry. From the present study, clearly the obtained optical properties of KNN thin films show that these films are potential candidates for application in optical devices and electro-optic modulators.

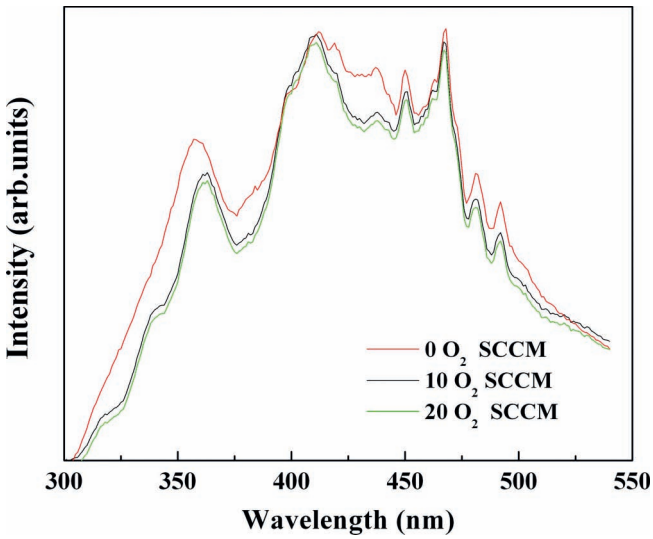

Fig. 6: PL spectra of annealed films deposited under different O_2 SCCM.

(4) Mechanical properties:

The variation in hardness and elastic modulus of the KNN films as a function of O_2 SCCM is shown in Fig. 7. It is observed that both the hardness and elastic modulus of the films are found to decrease with an increase in O_2 SCCM. Also the as-deposited films show higher values compared to the films annealed at 500 °C. Further, the hardness of the films is found to be 10.74 to 3.4 GPa and 7.23 to 1.54 GPa for the as-deposited and for the films annealed at 500 °C, respectively. The elastic modulus values are in the range of 80.3 – 30 and 68.3 – 17.8 GPa for the as-deposited and for the films annealed at 500 °C, respectively. It is significant to note that the values obtained for the hardness and the elastic modulus are comparable with the values reported in the literature [21, 25, 26]. The reduction in the elastic modulus and hardness values of the films with the increase in O_2 SCCM may be due to the increase in bond length between the metal and oxygen, the increase in average particle size/crystallite size and surface roughness,

which is observed from the SEM images and XRD patterns. Creep and thermal drift do not play major role in this case because the measurements were performed at ambient temperatures. Further, it is interesting to note that optical band-gap energy of the films as a function of O_2 SCCM showed similar behavior to the hardness and elastic modulus as a function of O_2 SCCM. Moreover, it is observed that with an increase in O_2 SCCM, the average crystallite size of the films increases and the SEM images also confirmed the similar behavior. This dependence shows that both the optical and mechanical properties of the KNN films are heavily influenced by the crystallinity, average particle sizes, O_2 SCCM and annealing temperature.

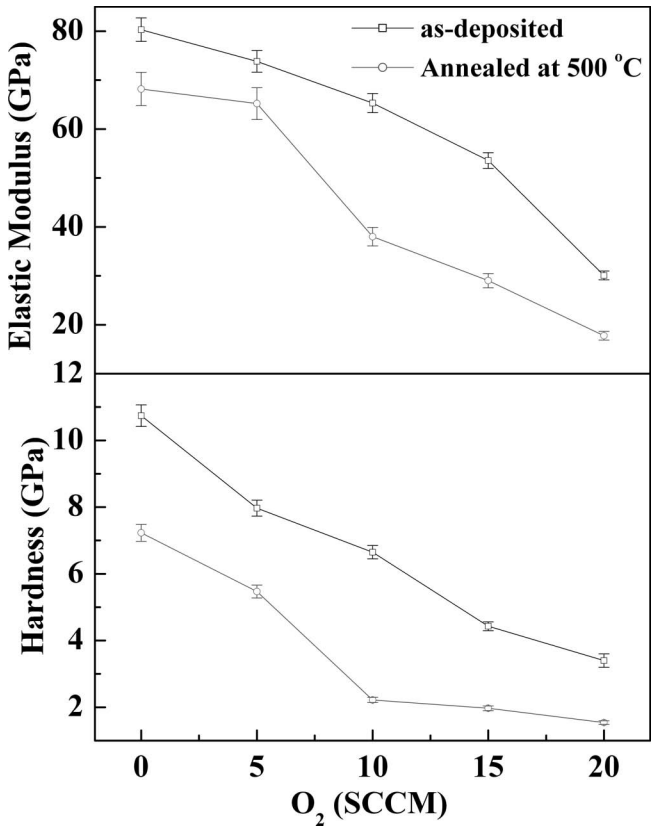

Fig. 7 : Variation of the elastic modulus and hardness of the KNN thin films deposited at ambient temperature and annealed at 500 °C as function of O_2 SCCM.

IV. Conclusions

Nanocrystalline $(K_{0.34}Na_{0.65})NbO_{3.01}$thin films were deposited on SiO_2 substrates by means of RF magnetron sputtering, and their optical properties reported for the first time. The as-deposited films were found to be amorphous and exhibited crystallinity on annealing at 500 °C. The refractive index and packing density of the films were found to increase whereas the band-gap energy decreased with an increase in O_2 SCCM. The enhancement in the refractive index of the KNN films was attributed to improvement in the crystallinity, packing density and microstructure of the films. The higher values obtained for the hardness and elastic modulus of the films grown in ambient temperature were attributed to the smaller particle sizes. It was observed that the post-annealing temperature and O_2 SCCM heavily influenced the structural, microstructural, optical and mechanical properties of KNN thin films.

Acknowledgements

The authors acknowledge the financial support from DAE-BRNS [2010/20/37P/14BRNS]. The facilities provided by DRDO [ERIP/ER/0900371/M/01/1264], BRFST [NFP-RF-A12 – 01] and DST [SR/FTP/PS-109/2009] are acknowledged.

References

1 Saito, Y., Takao, H., Tani, T., Nonoyama, T., Takatori, K., Homma, T., Nagaya, T., Nakamura, M.: Lead-free piezoceramics, *Nature,* **432**, 84 – 87, (2004).

2 Cross, E.: Lead-free at last, *Nature*, **432**, 24– 25, (2004).

3 Woolf, A.D., Goldman, R., Bellinger, D.C.: Update on the clinical management of childhood lead poisoning, *Pediatr. Clin. N. Am.,* **54,** 271 – 294, (2007).

4 Zhen, Y., Li, J.F.: Normal sintering of $(K,Na)NbO_3$-based Ceramics: influence of sintering temperature on densification, microstructure, and electrical properties, *J. Am. Ceram. Soc.,* **89,** 3669 – 3675, (2006).

5 Joshi, P.C., Mansingh, A., Kamalasanan, M.N., Subhas, C.: Structural and optical properties of ferroelectric $Bi_4Ti_3O_{12}$ thin films by sol gel technique, *Appl. Phys. Lett.,* **59,** 2389 – 2390, (1991).

6 Kato, K., Suzuki, K., Nishizawa, K., Miki, T.: Ferroelectric properties of alkoxy-derived $CaBi_4Ti_4O_{15}$ thin films on Pt-passivated si, *Appl. Phys. Lett.,* **78**, 1119 – 1121, (2001).

7 Buhay, H., Sinharoy, S., Kasner, W.H., Francombe, M.H., Lampe, D.R.: Pulsed laser deposition and ferroelectric characterization of bismuth titanate films, *Appl. Phys. Lett.,* **58**, 1470 – 1472, (1991).

8 Pontes, F.M., Leite, E.R., Pontes, D.S.L., Longo, E., Santos, E.M.S., Mergulhao, S., Pizani, P.S., Lanciotti, F. Jr., Boschi, T.M., Varela, J.A.: Ferroelectric and optical properties of $Ba_{0.8}Sr_{0.2}TiO_3$ thin film, *J. Appl. Phys.,* **91,** 5972 – 5978, (2002).

9 Bernard, J., Bencan, A., Rojac, T., Holc, J., Malic, B., Kosec, M.: Low-temperature sintering of $K_{0.5}Na_{0.5}NbO_3$ ceramics, *J. Am. Ceram. Soc.,* **91**, 2409 – 2411, (2008).

10 Li, N., Li, W.L., Zhang, S.Q., Fei, W.D.: Effect of post-annealing treatment in oxygen on dielectric properties of $K_{0.5}Na_{0.5}NbO_3$ thin films prepared by chemical solution deposition, *Thin Solid Films,* **519**, 5070 – 5073, (2011).

11 Harada, S., Muralt, P.: Pulsed laser deposition of KNN-based ferroelectric thin films on platinised si substrates, *IOP Conf. Ser.: Mater. Sci. Eng.,* **8,** 012004, (2010).

12 Tennery, V.J., Hang, K.W.: Thermal and X-ray diffraction studies of the $NaNbO_3$-$KNbO_3$ system, *J. Appl. Phys.,* **39,** 4749 – 753, (1968).

13 Mgbemere, H.E., Herber, R.P., Schneider, G.A.: Investigation of the dielectric and piezoelectric properties of potassium sodium niobate ceramics close to the phase boundary at $(K_{0.35}Na_{0.65})NbO_3$ and partial substitutions with lithium and antimony, *J. Eur. Ceram Soc.,* **29,** 3273 – 3278, (2009).

14 Zang, G.Z., Yi, X.J., Du, J., Wang, Y.F.: Co_2O_3 doped $(Na_{0.65}K_{0.35})NbO_3$ piezoceramics, *Mater. Lett.,* **64,** 1394 – 1397, (2010).

15 Swanepoel, R.: Determination of the thickness and optical constants of amorphous silicon, *J. Phys. E: Sci. Instrum.,* **16,** 1214 – 1222, (1983).

16 Bhuyan, R.K., Santhosh Kumar, T., Perumal, A., Ravi, S., Pamu, D.: Optical properties of ambient temperature grown nanocrystalline Mg_2TiO_4 thin films, *Surf. Coat. Tech.,* **221**, 196 – 200, (2013).

17 Cho, C.R., Grishin, A.: Background oxygen effects on pulsed laser deposited $Na_{0.5}K_{0.5}NbO_3$ films: from superparaelectric state to ferroelectricity, *J. Appl. Phys.,* **87,** 4439 – 4448, (2000).

18 Ahn, C.W., Hwang, H., Lee, K.S., Jin, B.M., Park, S., Park, G., Yoon, D., Cheong, H., Lee, H.J., Kim, W.: Raman spectra study of $K_{0.5}Na_{0.5}NbO_3$ ferroelectric thin films, *Jpn. J. Appl. Phys.,* **49**, 095801, (2010).

19 Feng, S., Li, G., Li, L., Li, X.: Hydrothermal synthesis and high pressure phase transition of impurity-stabilized cubic $KNbO_3$, *Rev. High Pressure Sci. Technol.,* **7**, 1362 – 1367, (1998).

20 Kim, B.Y., Seong, T.G., Seo, I.T., Jang, M.S., Nahm, S., Kang, J.Y., Yoon, S.J.: Effects of annealing atmosphere on the structural and electrical properties of $(Na_{0.5}K_{0.5})NbO_3$ thin films grown by RF magnetron sputtering, *Acta Mater.,* **60,** 3107 – 3112, (2012).

21 Kugler, V.M., Soderlind, F., Music, D., Helmersson, U., Andreasson, J., Lindback, T.: Low temperature growth and characterization of (Na,K)NbOx thin films, *J. Cryst. Growth*, **254**, 400 – 404, (2003).

22 Lee, H.J., Kim, I.W., Jin, B.M.: The effect of the substrate temperatures on $(Na,K)NbO_3$ ferroelectric thin films fabricated by RF magnetron sputtering, *J. Korean Phys. Soc.,* **56,** 417 – 420, (2010).

23 Yongsiri, P., Sukum, E., Gobwut, R., Somnuk, S., Tawee, T., Kamonpan, P.: Fabrication of transparent lead-free KNN glass ceramics by incorporation method, *Nanoscale Res. Lett.,* **7,** 136, (2012).

24 Tauc, J.C.: Optical properties of solids, North-Holland, Amsterdam, 1972.

25 Brunckova, H., Medvecky, L., Hvizdos, P.: Effect of substrate on microstructure and mechanical properties of sol-gel prepared (K, Na)NbO_3 thin films, *Mater. Sci. Eng. B,* **178,** 254 – 262, (2013).

26 Shibata, K., Suenaga, K., Nomoto, A., Mishima, T.: Curie temperature, biaxial elastic modulus, and thermal expansion coefficient of (K,Na)NbO_3 piezoelectric thin films, *Jpn. J. Appl. Phys.,* **48**, 121408, (2009).